Network resilience of FitzHugh-Nagumo neurons in the presence of nonequilibrium dynamics

Subhendu Bhandary,[1] Taranjot Kaur,[1] Tanmoy Banerjee,[2,*] and Partha Sharathi Dutta[1,†]

[1]*Department of Mathematics, Indian Institute of Technology Ropar, Rupnagar 140 001, Punjab, India*

[2]*Chaos and Complex Systems Research Laboratory, Department of Physics, University of Burdwan, Burdwan 713 104, West Bengal, India*

(Received 31 August 2020; accepted 1 February 2021; published 18 February 2021)

Many complex networks are known to exhibit sudden transitions between alternative steady states with contrasting properties. Such a sudden transition demonstrates a network's resilience, which is the ability of a system to persist in the face of perturbations. Most of the research on network resilience has focused on the transition from one equilibrium state to an alternative equilibrium state. Although the presence of nonequilibrium dynamics in some nodes may advance or delay sudden transitions in networks and give early warning signals of an impending collapse, it has not been studied much in the context of network resilience. Here we bridge this gap by studying a neuronal network model with diverse topologies, in which nonequilibrium dynamics may appear in the network even before the transition to a resting state from an active state in response to environmental stress deteriorating their external conditions. We find that the percentage of uncoupled nodes exhibiting nonequilibrium dynamics plays a vital role in determining the network's transition type. We show that a higher proportion of nodes with nonequilibrium dynamics can delay the tipping and increase networks' resilience against environmental stress, irrespective of their topology. Further, predictability of an upcoming transition weakens, as the network topology moves from regular to disordered.

DOI: 10.1103/PhysRevE.103.022314

I. INTRODUCTION

Biological systems are often composed of nonlinear interactions and may exhibit complex multistable dynamics in response to various stressors, such as biochemical changes, environmental fluctuations, etc. [1]. Empirical and theoretical evidences suggest that many multistable systems; including lakes [2], tropical forests [3], climate [4,5], cellular systems [6,7], and global finance [8] can undergo sudden transitions to alternative stable states [9]. These transitions occur when a system bypasses a critical value, known as a tipping point, due to the loss of resilience to perturbations [10–14]. Determining such sudden transitions is relatively easy when a species or an isolated system governs the state of a system. However, for complex networked systems where many nodes interact, e.g., genetic networks, neural networks, and ecological networks of interacting species—sudden transitions are highly unpredictable [15,16]. This is because current analytical frameworks of measuring resilience are mostly limited to low-dimensional systems and are underdeveloped for high-dimensional systems, where multiple components simultaneously interact through a complex network. Understanding, either the loss or the maintenance of network resilience in the face of internal disturbances or external environmental changes, is an important problem with broad interest.

Given a complex network, variations in the network topology can act as internal stress, which may perturb the system's resilience when exposed to stress deteriorating their external conditions (i.e., environmental stress) [17]. Factors disturbing network resilience have been studied in many contexts. For instance, in mutualistic interactions nodes can contribute heterogeneously in network resilience; removal of a strong contributor node can be more influential for species persistence than that of a weak contributor node [18]. In a plant-pollinator mutualistic network, the network architecture is known to drive a sudden collapse of pollinator species, and hence loss of network resilience [13,19]. Effects of climate change and anthropogenic factors on network resilience have been studied in Ref. [20]. Moreover, modifier genes can also maintain the resilience of gene interaction networks to perturbation [21]. Cascading failure of interdependent networks is investigated in Ref. [22]. Recently, analytical tools to understand and control resilience patterns of multidimensional systems have also been developed [15].

Real-world interactions are known to reveal diverse network architectures. Various social interactions, biochemical pathways, and protein-protein interactions primarily exhibit nonhomogeneous properties that often vary in degree distribution with the power-law formation or the scale-free interactions. Apart from diversity in network structure, the stability of complex networks is also accounted for damages in the network parameters such as changes in the number of links or nodes, coupling strength, average degree, etc. For example, Ref. [23] studied the robustness of communication networks to loss of nodes in the disintegration of the network from a well-functioning state to a disturbed state. Reference [24] investigated the resilience to damage the networks in graphs with degree correlations. Further, Refs. [25,26] suggested that strength up to which a system can adapt changes to external conditions can increase by introducing substantial heterogeneity, noise, or weak coupling amongst the connected components. However, Ref. [27] reported consideration of perfectly regular interaction to investigate network resilience

*tbanerjee@phys.buruniv.ac.in

†Corresponding author: parthasharathi@iitrpr.ac.in

[26] leads to bias in the outcomes. Nevertheless, the investigations mentioned above mostly neglect the role of complex local dynamics, while investigating the interplay between external stress and network topology in the occurrence of tipping points.

While investigating the resilience patterns of complex networks, for mathematical tractability, it is appealing to consider either one-dimensional or two-dimensional nonlinear systems in each node with equilibrium steady-state dynamics. However, this may overlook the concurrent effects of nonequilibrium dynamics preceding a transition [28]. Such nonequilibrium/cyclic dynamics may generate tradeoff among other nodes, which can further suppress or fuel the occurrence of tipping points in the interaction network. In dynamical systems, cyclic dynamics mostly occur due to negative feedback, and positive feedback generates hysteresis loops, which creates the possibility of sudden transition of an equilibrium steady state. It would be interesting to study the resilience of a heterogeneous network, where a fraction of its nodes can exhibit equilibrium steady state, and a fraction of nodes can show cyclic dynamics. This new direction bear relevance for the management of tipping points in many networks, like neuronal and ecological networks, where oscillations are ubiquitous.

Here we consider a network of FitzHugh-Nagumo (FHN) neurons [29,30]. The FHN model represents a paradigmatic neuronal model and have widely been used to study the collective behaviors of an ensemble of excitable as well as self excitatory spiking neurons. Several concepts of synchronization [31], coherence resonance [32], and chimera states [33] have been discovered using networks of FHN neurons. Some of the emergent dynamics have been believed to have connections with observable physiological and cognitive behaviors. For example, the so-called bump state was proposed as the mechanism behind the visual orientation tuning in the rat's brain [34]. The unihemispheric slow-wave sleep in aquatic mammals and some migratory birds is connected with the coherent-incoherent dynamics of coupled oscillating neurons [35]. Recently, it has been shown explicitly that FHN oscillators on complex networks mimic epileptic-seizure-related synchronization phenomena [36].

In this work, one of our main interests is to study the influence of diverse network topologies and environmental stress on the FHN network resilience in the presence of nonequilibrium dynamics [28]. We find that in a regular FHN network with heterogeneity in nodes, sometimes transitions from one stable state to another is gradual (i.e., continuous/second-order phase transition). At the same time, it can be sudden (i.e., discontinuous/first-order phase transition) for disordered networks. The management of internal parameters, such as coupling strength or average degree, can significantly influence the type of transitions. When the network is dominated by cyclic dynamics in proportion of nodes, an equilibrium network state precedes nonequilibrium dynamics. We find that a precise classification of transition type is not always possible. We observe fluctuations before a transition in both regular and disordered networks, under external stress, which indicates that the presence of nonequilibrium dynamics in a proportion of nodes plays a significant role in determining network resilience. Further, we find that the efficacy of covariance-based early warning signals weakens, as the network topology moves from regular to disordered.

II. MATHEMATICAL MODEL

A. A single FHN neuron

We consider the following model of the FHN neuron:

$$\frac{dx}{dt} = \frac{1}{\epsilon}\left(x - \frac{1}{3}x^3 - y\right), \tag{1a}$$

$$\frac{dy}{dt} = gx - y + b, \tag{1b}$$

where x is the membrane potential, and y is the recovery variable [37]. ϵ controls the time scale separation between the membrane potential (x) and the recovery variables (y) ($0 < \epsilon < 1$) [29]. The parameters b and g are the control parameter of the neuron: depending upon them each isolated FHN neuron can undergo several transitions between equilibrium and cyclic (or oscillating) dynamics. This transitions are governed by saddle-node bifurcation or/and Andronov-Hopf bifurcation.

For a clear understanding of the underlying dynamics of a single neuron, we resort to bifurcation diagrams with b for different values of g (see Fig. 1). For $g = 0.2$ ($\epsilon = 0.2$), with variations in b the model shows a bistable region consisting of the stable fixed point branch (solid line) and unstable fixed point branch (dashed line); the stable and unstable branches are governed by two saddle-node bifurcations denoted by SN [Fig. 1(a)]. For an increase in g, the stable branches lose their stability via a subcritical Andronov-Hopf bifurcation (HB) and thereby gives rise to an unstable limit cycle (blue filled circles): this is shown in Fig. 1(b) for an exemplary value $g = 0.6$. With a further increase in g, this unstable limit cycle gets stabilized through the saddle-node bifurcation of the limit cycle (SNLC) and as a result a stable limit cycle emerges (yellow filled circles): Figs. 1(c) and 1(d) show this scenario for $g = 0.8$ and $g = 1.0$, respectively. It can be seen that the width of the limit cycle region along the b-axis increases with increasing g. Another qualitative difference between Figs. 1(c) and 1(d) is the role of the unstable branch (dashed line); while in the former figure the unstable branch separates the phase space in four regions, in the latter case the number of separate region is two. Therefore, the bifurcation scenarios indicate that for higher g values the system experience sudden transitions from an equilibrium steady state to a nonequilibrium state (i.e., a limit cycle) and vice versa with the variation of b and the exact organization of the limit cycles is governed by the unstable branch.

B. Networks of FHN neuron

Next, we consider a network of FHN neurons [37–39] where dynamics of the ith neuron in a network of N neurons are governed as follows:

$$\frac{dx_i}{dt} = \frac{1}{\epsilon}\left(x_i - \frac{1}{3}x_i^3 - y_i\right) + \frac{d}{k_i}\sum_{j=1}^{N} A_{ij}(x_j - x_i), \tag{2a}$$

$$\frac{dy_i}{dt} = g_i x_i - y_i + b, \tag{2b}$$

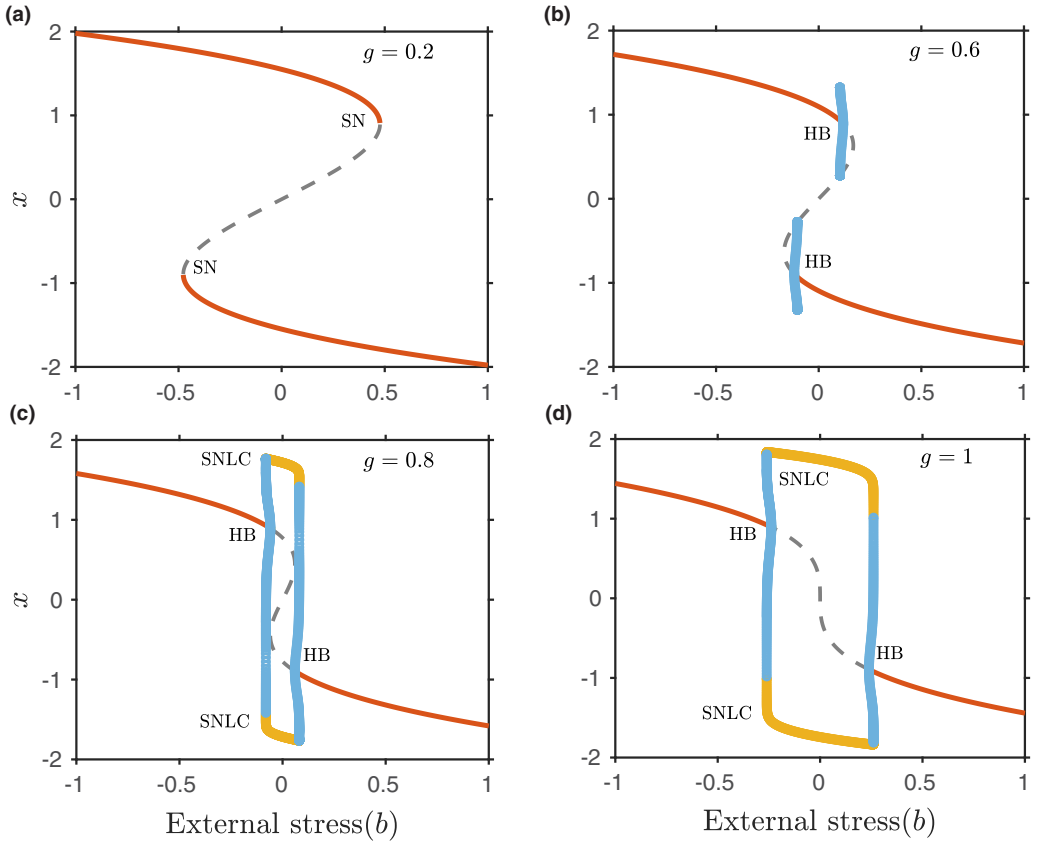

FIG. 1. One-parameter bifurcation diagrams of the FHN Eq. (1) along changing the parameter b: for (a) $g = 0.2$, (b) $g = 0.6$, (c) $g = 0.8$, and (d) $g = 1$. Solid lines and dashed lines represent stable and unstable steady states, respectively. Whereas yellow and blue filled circles represent stable and unstable limit cycles, respectively. Here, SN represents a saddle-node bifurcation point, HB represents a subcritical Andronov-Hopf bifurcation point, and SNLC represents a saddle-node bifurcation of the limit cycle. Other parameter value: $\epsilon = 0.2$.

where $i = 1, 2, \ldots, N$ denotes the node index and d is the interaction strength between neurons. The diffusive coupling incorporated in x_i allows transmission of signals from low to high potential, in various parts of a cell. A_{ij} is the element of the adjacency matrix (A) of the network, which is equal to 1 if nodes i and j are connected and 0 otherwise. k_i denotes the number of connections corresponding to the ith node ($k_i = \sum_{j=1}^{N} A_{ij}$). g_i is the parameter through which heterogeneity among the nodes can be introduced in the network, and b is considered as the external stress that drives the system to the transition point.

By simple algebraic manipulation we can rewrite Eq. (2) in terms of the Laplacian matrix (L) as follows:

$$\frac{dx_i}{dt} = \frac{1}{\epsilon}\left(x_i - \frac{1}{3}x_i^3 - y_i\right) - \frac{d}{k_i}\sum_{j=1}^{N} L_{ij}x_j, \tag{3a}$$

$$\frac{dy_i}{dt} = g_i x_i - y_i + b, \tag{3b}$$

where L_{ij} is the element of the Laplacian matrix, such that $L_{ii} = \sum_{j=1}^{N} A_{ij}$ and $L_{ij} = -A_{ij}$ for $i \neq j$. Here we consider three different network architectures; the Watts-Strogatz (WS) model [40], the Erdős-Rényi (ER) model [41], and the Barabási-Albert (BA) model [42]. For the WS model, the interaction networks are generated using a rewiring probability (p). This probability determines the randomness of connectivity in a network. For example, the network is regular for $p = 0$ with each node corresponds to same degree distribution, completely random when $p = 1$, and is small-world for $0 < p < 1$. The ER and BA models generate random and scale-free networks, respectively. However, the ER model follows Poisson distribution and the latter follows power-law distribution. For all the aforementioned interaction networks, without any loss of generality, the average degree is kept at $k = \frac{1}{N}\sum_{i=1}^{N} k_i = 4$, with k_i being degree of the ith node; also, we consider $N = 1000$ unless mentioned otherwise.

III. RESULTS

For numerical integration, we use the fourth-order Runge-Kutta method with adaptive step size and initial conditions (x_i, y_i) are randomly selected from $[-2, 2]\times[-2, 2]$. Throughout this paper we take $\epsilon = 0.2$.

To analyze the resilience of the FHN networks, we calculate the stationary state of the network Eq. (3). We define the network state as $X = \frac{1}{N}\sum_{i=1}^{N} x_i$. When $X > 0$ (i.e., positive membrane potential), the network exhibits a potential difference between the cell membranes. Thus, signals transmitted between different parts of the cell and the neuronal interactions are active. When $X < 0$ (i.e., negative membrane

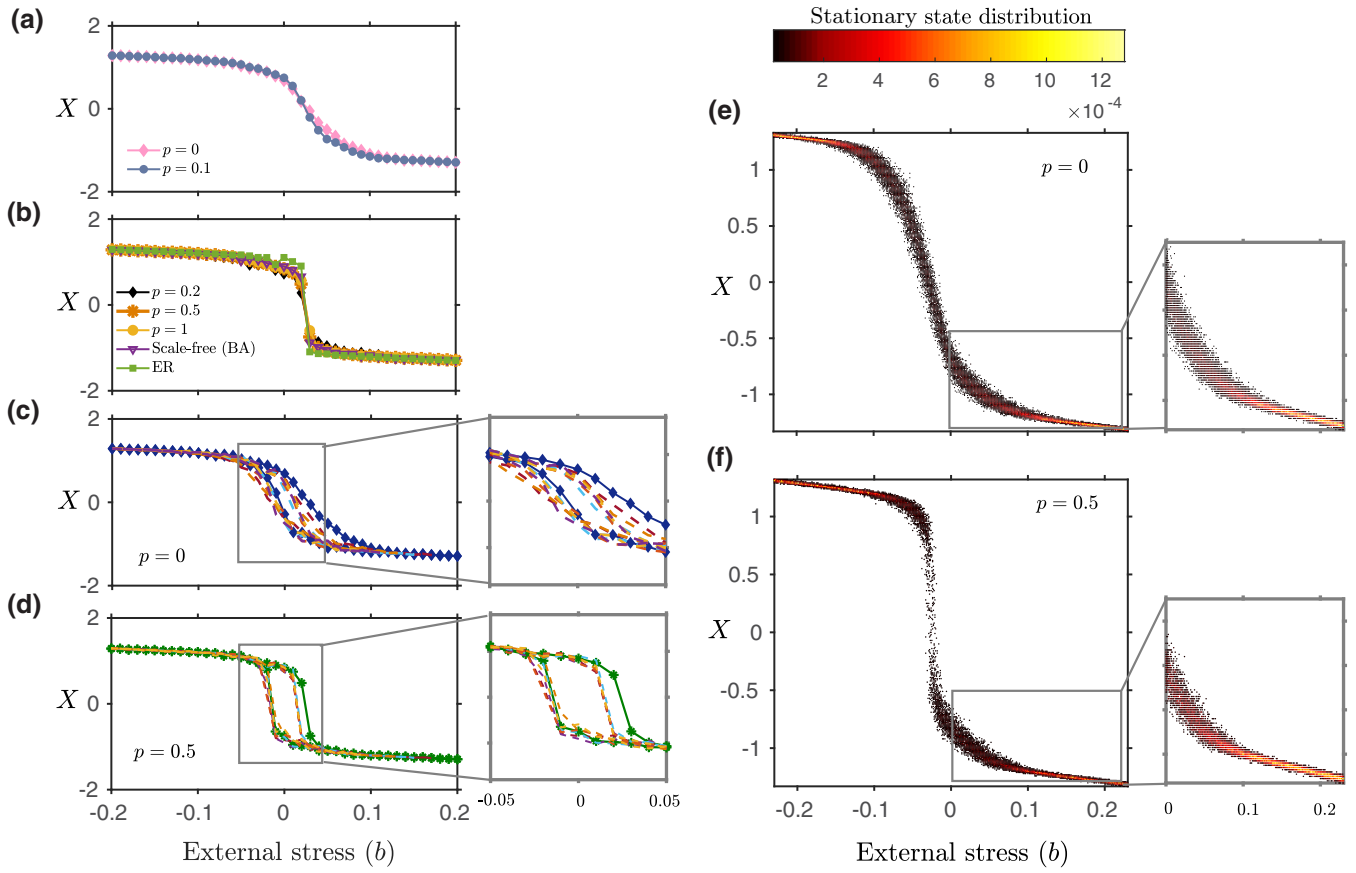

FIG. 2. Stationary state (X) of the FHN network with variations in b: for (a) regular ($p = 0$) and small world ($p = 0.1$) networks, (b) small world topology with $p = 0.2$ and p = 0.5, WS, BA, and ER networks. (c), (d) Each dashed line represents single realisation obtained by increasing the stress b from -0.3 and then decreasing the stress b once it reaches $b = 0.07$, $b = 0.09$, $b = 0.11$, $b = 0.13$, $b = 0.15$, and $b = 0.17$, for the WS network with $p = 0$ and $p = 0.5$. (e), (f) Stationary state distribution of regular network ($p = 0$), and small-world network ($p = 0.5$), respectively. The blow-up diagrams represent magnified dynamics observed for a range of b. To estimate the stationary state distribution of a network we generate 5×10^4 stationary states, where b is randomly selected from $[-0.2, 0.2]$ following uniform distribution, similarly g_i is randomly chosen from uniform distribution [0.2,1], and initial conditions (x_i, y_i) are randomly selected from $[-2, 2]\times[-2, 2]$. The other parameters are $\epsilon = 0.2$, and $d = 1.5$.

potential), the system is at the resting state. Here, stationary states are calculated as an average of 100 independent simulations.

A. Role of network topology on determining the nature of transitions

We identify the role of network topology in response to the external stress (b) by obtaining the stationary network state X for the WS, ER, and BA models. The stationary state X is calculated by increasing the stress b from -0.3 to 0.3 with an increment of $\delta b = 0.01$ and g_i is randomly chosen from [0.2,1] with a uniform distribution. We take the coupling strength $d = 1.5$. Figure 2 depicts the response of the network with different rewiring probability (p) of the WS model, varying from a perfectly regular network to a completely random network via the small-world networks. For low stresses, each network exhibits an active state while moving to a resting state as b increases beyond a critical threshold. However, the nature of the transition from an active to a resting state depends upon the network topology. Regular networks reveal gradual response to the stress [Fig. 2(a)], which is a hallmark of second-order phase transition [25,26]. However, disordered networks (WS networks with $p \geqslant 0.2$, the ER and the BA networks) exhibit an abrupt transition from $X > 0$ to $X < 0$ [see Fig. 2(b)] a true discontinuous, first-order phase transition.

Further, we investigate the occurrence of hysteresis loops in the network when the external stress b is decreased from $b = 0.3$ to $b = -0.3$ [Figs. 2(c) and 2(d)]. We find that hysteresis loops occur for both the continuous and the discontinuous transitions. Each pathway of X corresponds to increasing the stress b from -0.3 and then decreasing it once the stress reaches to $b = 0.07$, $b = 0.09$, $b = 0.11$, $b = 0.13$, $b = 0.15$, and $b = 0.17$. Since all the pathways of transition from one state to another in both the scenarios are comparable, it suggests no strategy to mitigate the hysteresis in networks by controlling the external parameter b in the WS networks (regular to disordered behavior). Thus, we find the transition threshold and changing environmental stress associated with tipping points in disordered networks, which can lead to a catastrophic transition. However, for regular networks, a transition from active to resting-state or vice-versa is not characterized by a tipping point.

To elucidate the nature of the transition thresholds, we generate stationary state distributions of Eq. (3), with different network topologies. A large number of stationary states are estimated to construct the stationary state distributions. We generate 5×10^4 stationary states (X's), where values of b are randomly selected from the interval $[-0.2, 0.2]$ following the uniform distribution, initial conditions (x_i, y_i) are randomly selected from $[-2, 2]\times[-2, 2]$, and g_i is also randomly selected from [0.2,1] following the uniform distribution. The stationary state distribution of the regular network differs qualitatively to the transition type viz a viz disordered networks [see Figs. 2(e) and 2(f)]. A higher probability of stationary states is distributed in the active ($X > 0$) and resting ($X < 0$) states for both the regular and the disordered networks. Within the transition regions between two states, stationary states are dense for regular networks [Fig. 2(e)], while it becomes scattered for the disordered networks [Fig. 2(f)]. This implies that the transition in regular networks is continuous. Simultaneously, the stationary state distribution depicts a sudden jump from an upper to a lower state as randomness in network topology increases. Thus, regular networks have a higher degree of resilience to environmental perturbations than that of disordered networks. Overall, network topology significantly decides the nature of a system's transition in virtue of external stress. The state curve depicts gradual response for regular networks and abrupt change for disordered ($p \geqslant 0.2$), scale-free, and ER networks.

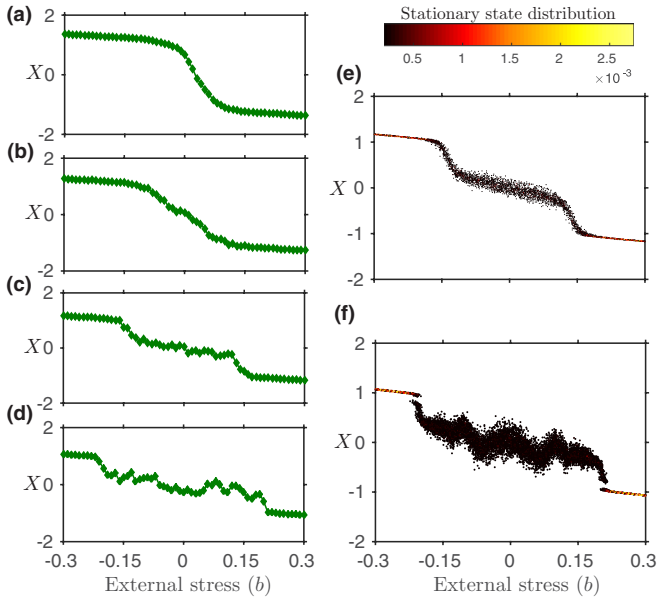

FIG. 3. Stationary states (X) of the regular network ($p = 0$) with changes in b, where g_i's are chosen from different intervals. g_i's are randomly chosen, following the uniform distribution, from the intervals: (a) $g_i \in [0.2, 1]$, (b) $g_i \in [0.4, 1]$, (c) $g_i \in [0.6, 1]$, and (d) $g_i \in [0.8, 1]$. Stationary state distributions of the network when: (e) $g_i \in [0.6, 1]$, and (f) $g_i \in [0.8, 1]$. The initial conditions and other parameters are the same as described in the caption of Fig. 2.

B. Effects of node heterogeneity

In this section, we study effects of different ranges of heterogeneity g_i on the network resilience for diverse network topologies, when exposed to external stress b. Figure 3 depicts the state curves for regular networks ($p = 0$) considering different ranges of g_i keeping the set of initial conditions and other network parameters fixed. As the range of g_i gets narrow (i.e., weak heterogeneity), we observe the significant influence of the limit cycle oscillations present in an isolated FHN neuron [see Figs. 1(c)–1(d)], during the transition in the network. When $g_i \in [0.2, 1]$ [Fig. 3(a)] and $g_i \in [0.4, 1]$ [Fig. 3(b)], there exists continuous transition like a transition from $X > 0$ to $X < 0$; however, the transition looks relatively flattered for the latter case. Further decrease in the heterogeneity range ($g_i \in [0.6, 1]$ and $g_i \in [0.8, 1]$) flattens the state curve near the transition threshold [Figs. 3(c) and 3(d)] and it becomes difficult to decide the nature of the transition. Since the dynamics of a few uncoupled neurons have limit cycle oscillations, to identify the significance of the cyclic dynamics on the network, we calculate the distribution of the stationary states when $g_i \in [0.6, 1]$ [Fig. 3(e)] and $g_i \in [0.8, 1]$ [Fig. 3(f)]. The stationary state distributions reveal a cluster of states in the vicinity of the transition thresholds. However, in the intermediate transition region, the stationary states get more scattered as the heterogeneity becomes weak (i.e., when we choose g_i from a narrow interval). This suggests that the networks with weak heterogeneity in g_i are more resilient as sudden transitions seem impossible. Therefore, the presence of limit cycle oscillations influences the network's resilience by inducing intermediate fluctuating stationary states as the network transits from an active to a resting state. Figure 4 depicts the proportion of nodes which are initially ($d = 0$) either in upper steady state or with cyclic dynamics, or in lower steady state with variations in the stress b and the interval in which g_i lies. The intermediate ranges of b, the 1000 nodes are in different states due to the variations in g_i. It is evident that when the network reaches its stationary state, the proportion of node dynamics alters from its initial configuration.

Next, we analyze the impact of cyclic dynamics for the disordered small-world network ($p = 0.5$). The stationary state curves depict that weakening of the heterogeneity parameter from $g_i \in [0.2, 1]$ to $g_i \in [0.4, 1]$ can suppress the sudden transition in the network and increase the resilience to the stress [see Figs. 5(a) and 5(b)]. Moreover, the cyclic dynamics' influence becomes more evident in the small-world network than the regular network. As b moves from a negative to a positive value, we initially see that the state $X(> 0)$ slowly approaching towards the transition point; however, the states are largely scattered before the transition to $X < 0$ in the intermediate region. Here, large fluctuations between the two states characterize transitions [see Figs. 5(c) and 5(d)]. Thus, small-world network topology switches the network state between alternative states before it reaches a resting state. The stationary state distributions of the network also reveal a strong influence of the cyclic dynamics in inhibiting large fluctuations between the active and the resting state [Figs. 5(e) and 5(f)]. Hence, heterogeneity in g_i can serve as a significant factor in determining the type of transition in the network.

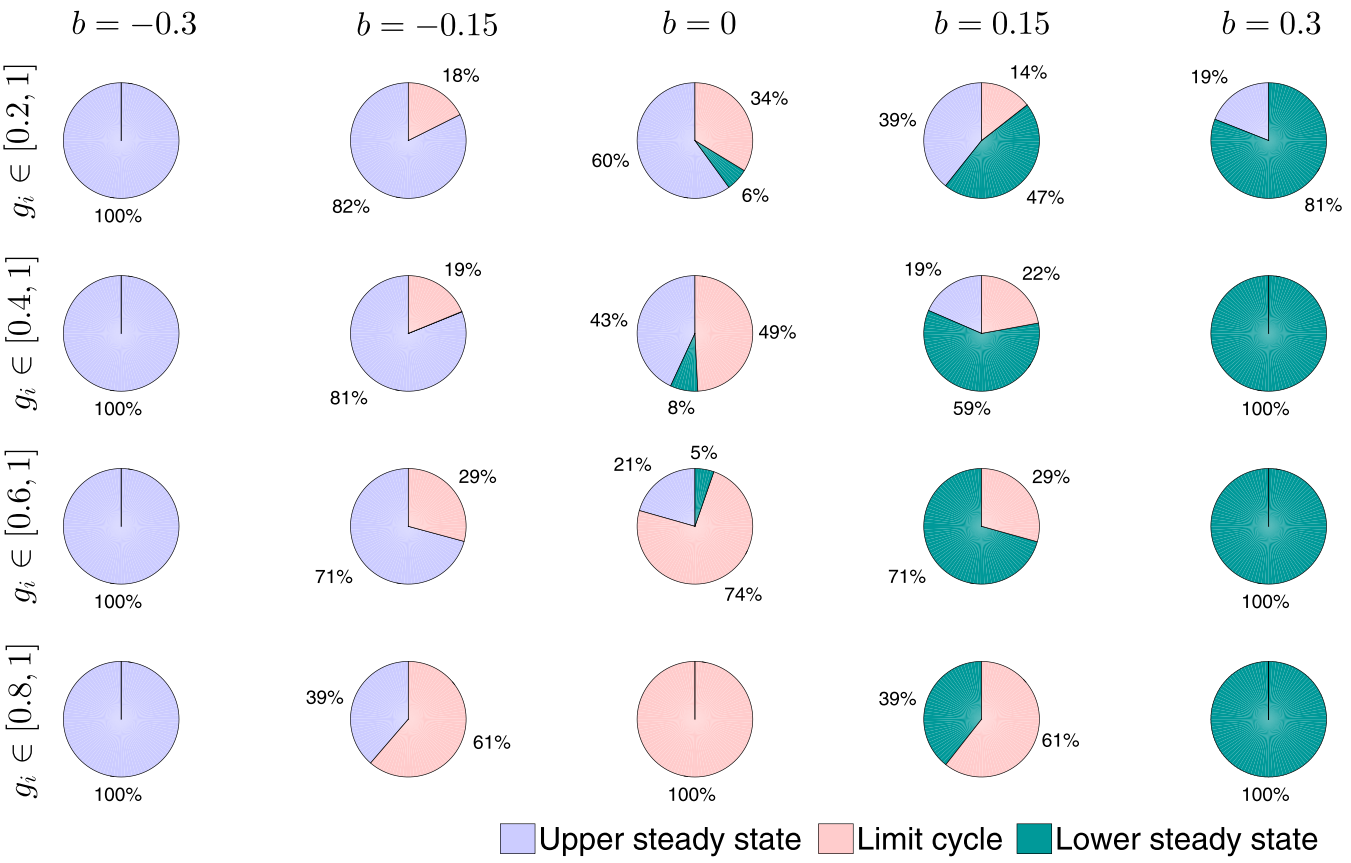

FIG. 4. Pie diagrams, when $d = 0$, representing the percentage of nodes exhibiting steady-state and cyclic dynamics, for different values of b and range of heterogeneity g_i. We consider an ensemble average of 100 realizations for each of the pie diagrams.

C. The role of network parameters

This section focuses on investigating the impact of network parameters, such as interaction strength (d) and average degree (k) on the resilience of the network (3) to the stress b. We observe the influence of the network topology and the cyclic dynamics on the resilience patterns, in Secs. III A and III B. Here, we calculate stationary state curves for different interaction strength (d), each for the regular and the disordered (small-world) networks as well as for different choice of the heterogeneity parameter g_i (Fig. 6). In particular, to isolate the impact of cyclic dynamics and d on the resilience of the network, we analyze the stationary state curves when $g_i \in [0.2, 1]$ [Figs. 6(a)–6(c)], and $g_i \in [0.6, 1]$ [Figs. 6(d)–6(f)].

We find that the resilience of regular and small-world networks with substantial heterogeneity ($g_i \in [0.2, 1]$) decreases as d increases. For the weak interaction strength $d = 0.5$, the type of transition is robust to network topology choice. In particular, we see continuous or second-order phase transitions [Fig. 6(a)]. However, the network tends toward an abrupt transition as d increases [Figs. 6(a)–6(c)]. Therefore, in the case of substantial heterogeneity in g_i, an increase in d can reduce adaptive responses to stress and trigger sudden collapse to the resting state, irrespective of the network topology. Further, regular networks experience a relatively smooth transition to external stress for $g_i \in [0.6, 1]$, while disordered networks show an increase in fluctuating states around transition thresholds with an increase in d. Therefore, when $g_i \in [0.6, 1]$ for large enough d, it is not possible to determine the transition type of the stationary state. They are neither first-order nor second-order transition.

Similarly, an increase in the network's average degree k leads to more stronger abrupt transition from one state to another for the system with strong heterogeneity ($g_i \in [0.2, 1]$), in case of both $p = 0$ and $p = 0.5$ [Figs. 7(a)–7(c)]. Note that changes in the network topology do not alter the system's response to b for high average degrees and strong heterogeneity in the system. For $g_i \in [0.6, 1]$, increase in k for both the network topologies leads to strong fluctuations prior to a transition to a resting state [Figs. 7(d)–7(f)]. Moreover, the fluctuations observed here for $p = 0.5$ are relatively stronger than those observed for $p = 0$ [Figs. 6(d)–6(f)]. Therefore, an increase in k and incorporating weak heterogeneity makes it difficult to determine the transition type. Overall, strong heterogeneity in g can improve networks' resilience with a low average degree and low coupling strength, while weak heterogeneity increases networks' resilience with strong d and k.

To check the stationary state of each node x_i, $i = 1, 2, \ldots, 1000$ for different interaction strengths d and external stress b, we calculate the percentage of nodes those exhibit either steady-state or cyclic dynamics (see Fig. 8). When the stress is close to the transition threshold ($b = 0$), we observe that for each isolated node ($d = 0$), the system is dominated by steady-state dynamics [Fig. 8(a)]. An increase in d leads to an oscillatory state in a large number of nodes [Figs. 8(b) and

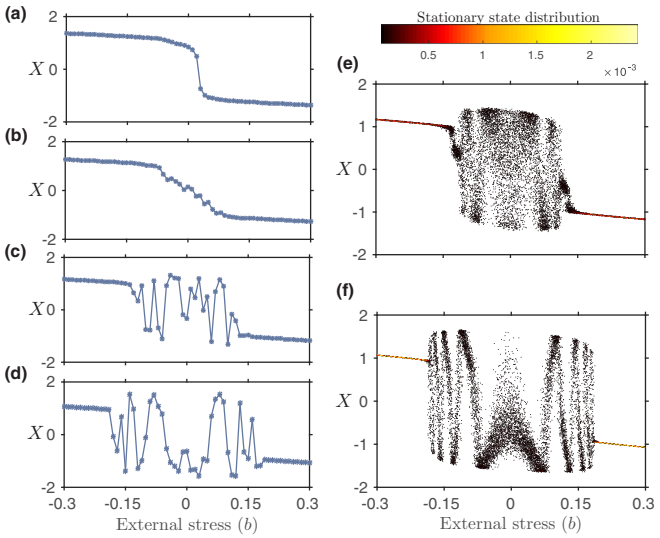

FIG. 5. Stationary states (X) of a disordered network ($p = 0.5$) with changes in b, where g_i's are randomly chosen, following the uniform distribution, from the intervals: (a) $g_i \in [0.2, 1]$, (b) $g_i \in [0.4, 1]$, (c) $g_i \in [0.6, 1]$, and (d) $g_i \in [0.8, 1]$. Stationary state distributions of the network when: (e) $g_i \in [0.6, 1]$, and (f) $g_i \in [0.8, 1]$. The initial conditions and other parameters are the same as described in the caption of Fig. 2.

8(c)], which further shows only oscillatory dynamics in all the nodes as d becomes very high [Fig. 8(d)]. Hence, when d is low, some nodes exhibit steady-state behavior while others fluctuate between active and resting states. The above results can lead to two exciting outcomes: First, if the steady state of the nodes represents their presence at an upper attractor, then a large number of nodes exhibit functional stability. An increase in d decreases the network's functional stability as all the nodes have changed their state from an upper attractor to an oscillatory state between the two attractors. Similarly, suppose the steady state for $d = 0$ represents the nodes are at resting state. In that case, an increase in d will enhance the functional stability as many nodes have shifted from a completely resting state to fluctuate between active and resting states.

The outcome is different for a negative value of the stress ($b = -0.15$), which is away from the transition threshold (Fig. 8). Initially ($d = 0$), steady states are dominating a majority of the nodes. As d increases, the percentage of cyclic states reduce, and finally, for large enough d dynamics in all the nodes become a steady state [Figs. 8(e)–8(g)].

D. Role of network topology on predictability of state transition

Analyses of diverse network topologies have shown different system responses while exhibiting transition from an active to a resting state. The regular network reveals a gradual transition of the FHN neurons network from an active state, transmitting signals to different parts of cells, to a resting state. However, this transition is sometimes discontinuous, giving rise to the tipping point in small-world interactions for $p = 0.2$ and beyond, BA and ER networks. Also, we observe fluctuating dynamics in the system with weak heterogeneity before an actual transition takes place. Thus, it is interesting to know how different transition mechanisms (gradual, abrupt, oscillatory), or in other words degree distribution of the networks affect the strength of predictability of state transitions in spatial interactions.

In many systems, a transition from a stable state to an alternative state preceded by a decrease in the equilibrium state's resilience. Studies suggest various statistical methods due to critical slowing down to anticipate transitions that occur in natural systems. In spatial models, critical slowing down is preceded by an increase in the state variable's spatial correlation and can serve as an early warning signal. Hence, it leads to an increase in fluctuations in the state variable, influencing fluctuations in the nearby state variables, leading to a more significant correlation in neighboring components. Here, we investigate the impact of network architecture; in other words, different transition types on the early warning indicator of spatial systems.

Consider a general form of a deterministic framework followed by stochastic perturbations [43,44]:

$$d\mathbf{z}(t) = f(\mathbf{z}(t), b)dt + DdW(t), \tag{4}$$

where deterministic part of the system is expressed as a vector function $\mathbf{f} = \{f_1, f_2, f_3, \ldots, f_N\}$ and state of the system $\mathbf{z}(t) = \{z_1(t), z_2(t), \ldots, z_N(t)\}$ is controlled by the dynamics of Eq. (4). $W(t)$ is a Wiener process with D as the noise intensity. Consider a vector of small deviation in the state $\mathbf{u} = \mathbf{z} - \mathbf{z}^*$, where $\mathbf{z}^*$ is the equilibrium point in the absence of any perturbation. Local stability of the fixed point $\mathbf{z}^*$ is calculated from the linearization of the perturbed differential equation:

$$\frac{d\mathbf{z}}{dt} = \frac{d\mathbf{u}}{dt} = \mathbf{f}(\mathbf{z}) = \mathbf{f}(\mathbf{z}^* + \mathbf{u}) \approx \mathbf{f}(\mathbf{z}^*) + J\mathbf{u} = J\mathbf{u}, \tag{5}$$

where J is the Jacobian matrix that determines the expected trajectory of the perturbed state as it returns to its equilibrium state z^*. Consider a probability distribution function $\rho(\mathbf{u}, t)$ to be a solution of (4) which can be approximated as a solution of the below linear Fokker Planck equation [45]:

$$\frac{\partial \rho(\mathbf{u}, t)}{\partial t} = -\sum_{i,j=1}^{N} J_{ij} \frac{\partial(\rho u_i)}{\partial u_i} + \frac{1}{2} \sum_{i,j=1}^{N} D_{ij} \frac{\partial^2 \rho}{\partial^2 u_i}. \tag{6}$$

The correlation between two state variables can be determined by a covariance matrix, where the diagonal elements represent fluctuations at each node and off-diagonal entries represent fluctuations between pair of nodes. The covariance matrix C can be written as [46]

$$C = -J^{-1}(D + Q)/2, \tag{7}$$

where Q is an antisymmetric matrix that can be estimated as

$$JQ + QJ^T = JD - DJ^T, \tag{8}$$

where the superscript T denotes the transpose of a matrix.

Near the bifurcation/tipping threshold, the dominant eigenvalue of the Jacobian matrix J tends to zero, and the eigenvector corresponding to the dominant eigenvalue will become slower. The rate at which the covariance matrix's dominant eigenvalue converges to zero is relatively faster than those of the other eigenvalues. Thus, the dominant eigenvalue

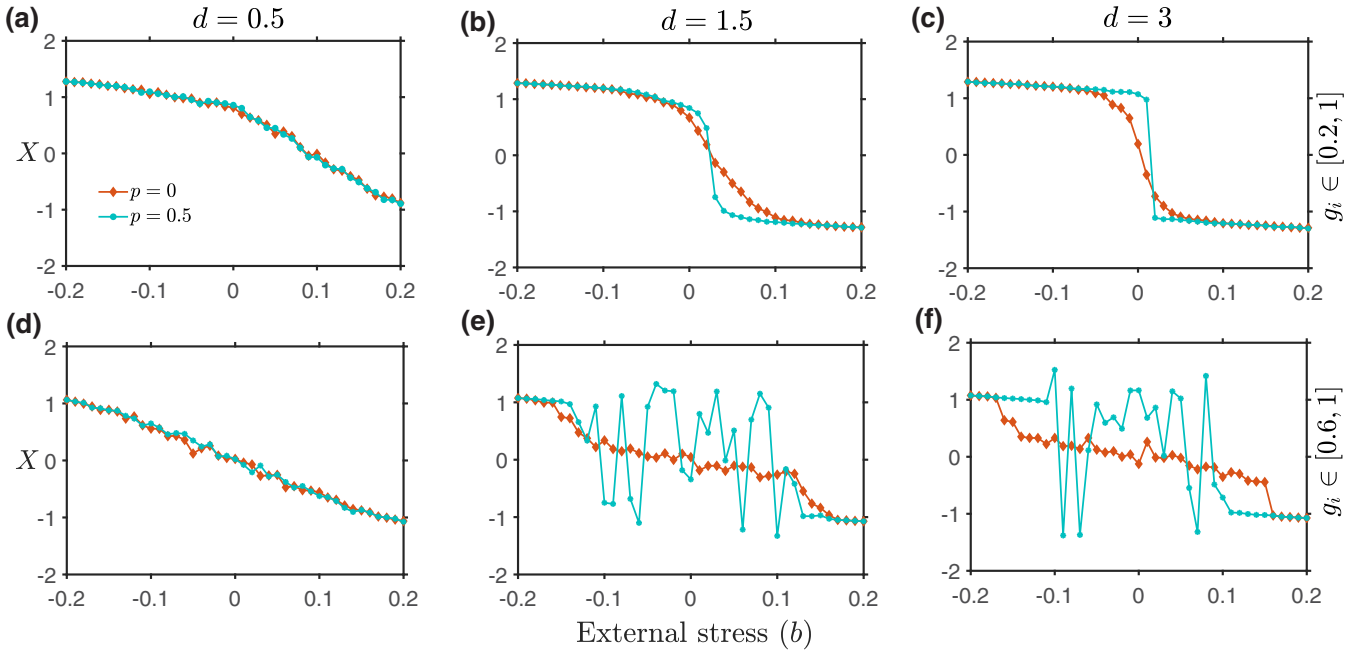

FIG. 6. The effect of different interaction strengths d on network resilience for both the regular and disordered networks with changes in b: for (a)–(c) $g_i \in [0.2, 1]$ and (d)–(f) $g_i \in [0.6, 1]$. The influence of cyclic dynamics becomes evident when heterogeneity in g_i becomes weak. The initial conditions and other parameters are the same as described in the caption of Fig. 2.

and its ratio over the Euclidean norm of a vector consisting of all eigenvalues of the covariance matrix serve as an early warning indicator in spatial interactions [47].

We begin our investigation by considering **f** as the deterministic FHN network Eq. (3) with N nodes. Each node has $\mathbf{z} = \{x_1, y_1, x_2, y_2, \ldots x_N, y_N\}$ as the pairwise potential and

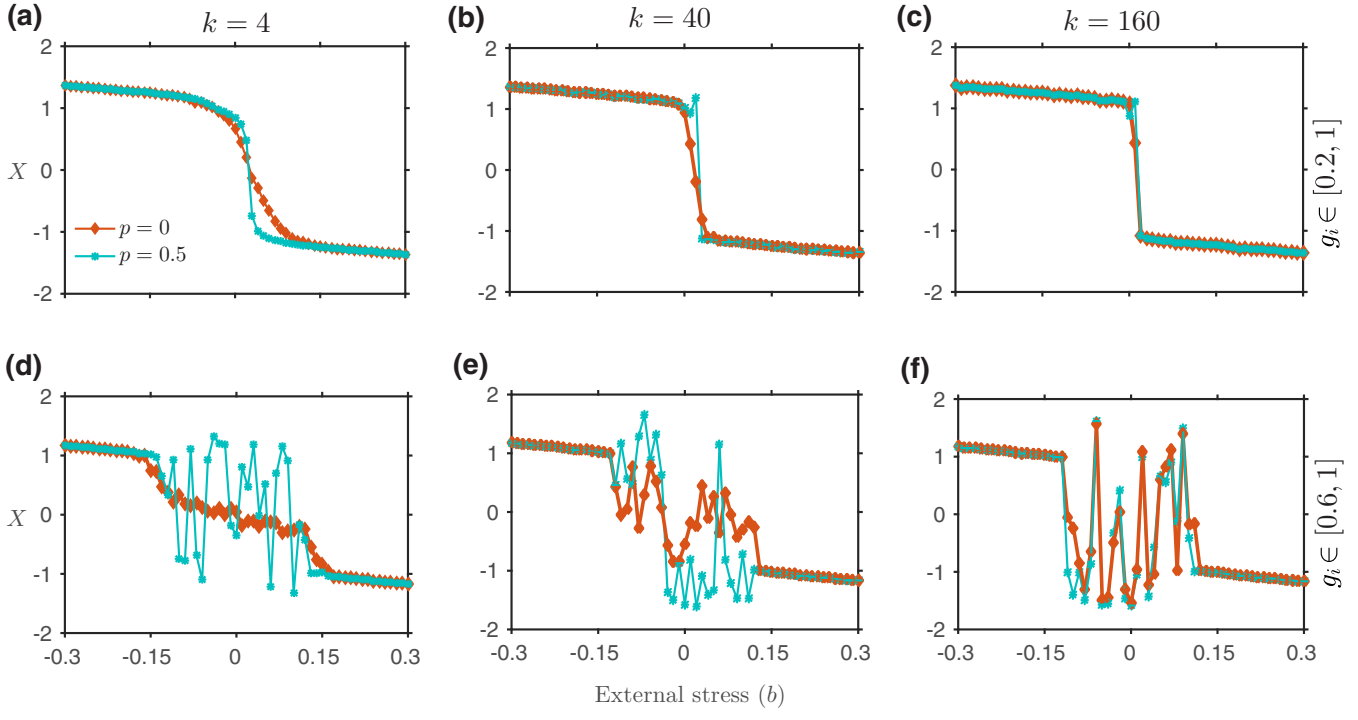

FIG. 7. The effect of different average degree k on network resilience for both the regular and disordered networks with changes in b: for (a)–(c) $g_i \in [0.2, 1]$ and (d)–(f) $g_i \in [0.6, 1]$. The influence of cyclic dynamics becomes evident when heterogeneity in g_i becomes weak. The initial conditions and other parameters are the same as described in the caption of Fig. 2.

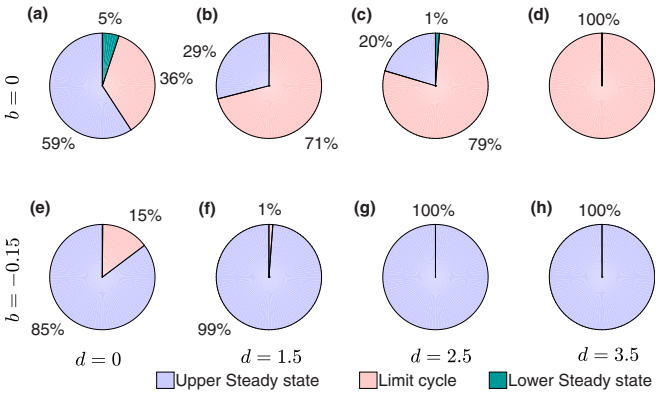

FIG. 8. Pie diagrams representing the percentage of nodes exhibiting steady-state and cyclic dynamics, for different values of d in a regular network: for (a)–(d) $b = 0$ and (e)–(h) $b = -0.15$. The initial conditions (x_i, y_i) are randomly chosen following uniform distribution from $[-2, 2]\times[-2, 2]$ with $d = 0$, and then we calculate the proportion of nodes exhibiting steady-state and oscillatory dynamics after removing the transients. For increasing values of d, the initial conditions used are same as for the system with no coupling ($d = 0$). We consider ensemble average of 100 realisations for each of the pie diagram.

recovery variables, respectively. Therefore, Eq. (4) can be expressed as

$$dz_{2i-1} = dx_i = \left(\frac{1}{\epsilon}\left(x_i - \frac{x_i^3}{3} - y_i\right) - \frac{d}{k_i}\sum_{j=1}^{N} L_{ij}x_j\right)dt + \sigma dW_i, \tag{9a}$$

$$dz_{2i} = dy_i = (g_i x_i - y_i + b)dt + \sigma dW_i, \tag{9b}$$

where $\sigma I = D$ and $\sigma = 0.01$ represents the noise intensity of each node. We generate the stochastic time series of the FHN network along changing external stress b, having both strong [Figs. 9(a)–9(c)] as well as weak heterogeneity [Figs. 9(d)–9(f)] in g_i, using Eq. (9). The stochastic time series along changing external stress, for each neuron (x_i) [Figs. 9(a) and 9(b)] reveals transition from active to resting state. Furthermore, the stationary state (X) stochastic time series reveals that this transition is relatively gradual for low rewiring probability of the network [Fig. 9(c)]. Investigating the stochastic time series for network with weak heterogeneity ($g_i \in [0.8, 1]$) depicts significant role of oscillatory dynamics in the state of each node [Figs. 9(d) and 9(e)]. We observe that the oscillation exhibit high amplitudes and demonstrate large fluctuations between alternative stable states for the small-world to completely random network. However, smaller fluctuations are identified when the network is perfectly regular [Fig. 9(f)]. Further, we calculate eigenvalues of the covariance matrix [using Eqs. (7) and (8)] of the stochastic system, where the Jacobian matrix J is given by

$$J_{2i-1,2j-1} = \begin{cases} \frac{1}{\epsilon}(1 - x_i^2) - \frac{d}{k_i}L_{ij}|_{z=z^*}, & \text{if } i = j, \\ \frac{d}{k_i}, & \text{if } i \neq j, \text{ and } i, j \text{ are connected}, \\ 0, & \text{if } i \neq j, \text{ and } i, j \text{ are not connected}, \end{cases}$$

$$J_{2i-1,2j} = \begin{cases} -1, & \text{if } i = j, \\ 0, & \text{if } i \neq j, \end{cases}$$

$$J_{2i,2j-1} = \begin{cases} g_i, & \text{if } i = j, \\ 0, & \text{if } i \neq j, \end{cases}$$

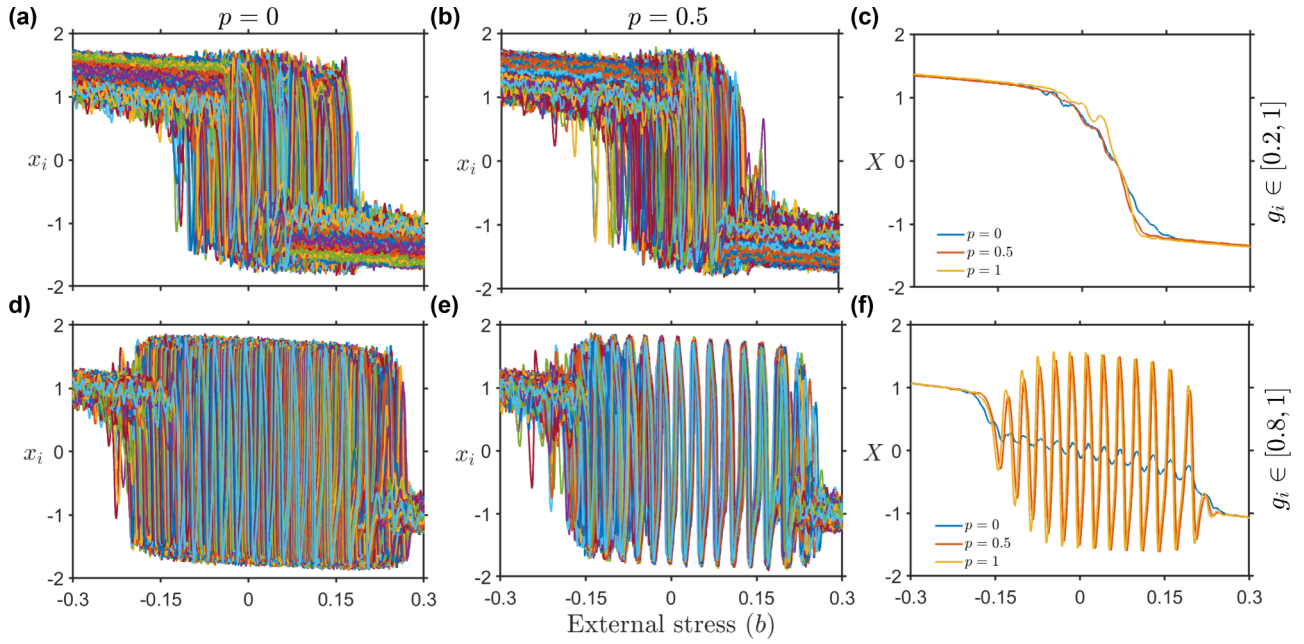

FIG. 9. Stochastic time series of the FHN neuron model [Eq. (9)] for different network topology and heterogeneity in g. (a), (b) Each line represents the time series of the potential variable at each node, when the network follows strong heterogeneity in g and has perfectly regular and small-world topology ($p = 0.5$), respectively. (c) Stationary state time series for the WS network with $p = 0$, $p = 0.5$ and $p = 1$. (d), (e) stochastic time series of each node when the heterogeneity become weak, that is, g_i is chosen randomly from uniform distribution [0.8,1]. (f) stochastic time series of the stationary state of the interaction network with weak heterogeneity.

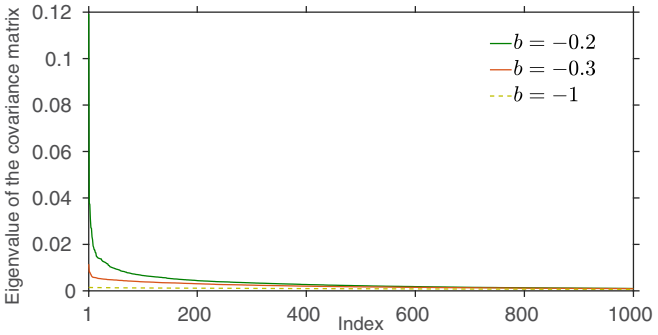

FIG. 10. Spectrum of the covariance matrix as the system (for $p = 0$) approaches close to the transition threshold. Each line represents the eigenvalues of the covariance matrix changes for different parametric values of the stress b. The Index i represents the index of ith eigenvalue corresponding to the potential variable of the network, when each eigenvalue is arranged in descending order.

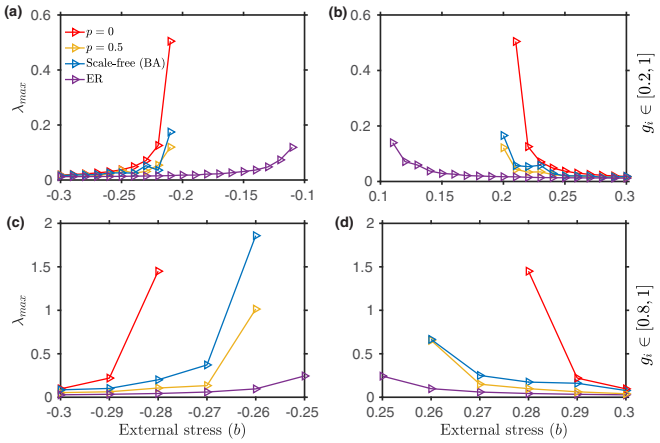

FIG. 11. Largest eigenvalue $\lambda_{\max}$ of the covariance matrix along with changes in the parameter b for different network structures, viz. completely regular ($p = 0$), small-world ($p = 0.5$), scale-free and Erdős-Rényi. (a), (b) g_i is randomly selected from uniform distribution [0.2,1]. (c), (d) g_i is randomly selected from uniform distribution [0.8,1].

and

$$J_{2i,2j} = \begin{cases} -1, & \text{if } i = j, \\ 0, & \text{if } i \neq j. \end{cases}$$

Let $\lambda_{\max} = \lambda_1 \leqslant \lambda_2 \leqslant \cdots \leqslant \lambda_{1000} = \lambda_{\min}$ be the eigenvalues corresponding to the potential variable of the covariance matrix C. Index is the integer varying from 1 to 1000 such that Index-1 denotes the index of largest eigenvalue, Index-2 corresponds to the index of second largest eigenvalue, and so on. We observe that the dominant eigenvalue (Index-1) of C increases at a larger rate than the other eigenvalues. Also, the difference between the dominant eigenvalue and other eigenvalues increases as the system approaches close to the transition threshold (Fig. 10). Thus, the dominant eigenvalue serves as an early warning indicator for the network. To investigate the role of different network topologies in predictability of the transition, we analyze the trend in the dominant eigenvalue of the covariance matrix along with the increasing/decreasing the stress b (Fig. 11). We observe that as the network approaches in the vicinity of the transition point, the dominant eigenvalue shows an increasing trend [Figs. 11(a) and 11(b)]. In case of weak heterogeneity, an increase in the largest eigenvalue is observed at relatively low value of b [Figs. 11(c) and 11(d)]. This is due to fluctuations preceded by the state of the system before the transition happens. Importantly, we notice that the indicator (as estimated by the dominant eigenvalue) works for all the regular, scale-free, small-world ($p = 0.5$) and ER networks, for both strong as well as weak heterogeinity in g. However, depending on the network topology the rise in $\lambda_{\max}$ varies. This suggests that the strength of predictability of an upcoming transition can depend upon the network topology.

IV. CONCLUSIONS AND DISCUSSION

Dynamical transitions from one stable state to another alternative stable state are hallmarks of loss of resilience in many complex systems [10,11,48]. Studies provide a myriad of mechanisms that lead to the occurrence of such transitions. These mechanisms propel the transition to an alternative stable state when an input condition bypass a critical point [3,49,50]. For instance, change in population growth due to reduced population size, changes in interaction strength between spatially connected components, etc. However, it has been challenging to understand how mechanisms altering the static dynamics of complex networks affect the occurrence of catastrophic and noncatastrophic transitions. Here, we aim to uncover, together with the presence of equilibrium dynamics, how nonequilibrium/cyclic dynamics in a few nodes of a network influence its resilience. We find that the proportion of uncoupled nodes exhibiting nonequilibrium dynamics plays a crucial role in determining the transition type of the network. A higher proportion of nodes with nonequilibrium dynamics can delay the tipping by inducing flickering between alternative network states against environmental stress, irrespective of their topology. Moreover, the predictability of a forthcoming transition weakens, as the network topology moves from regular to disordered.

Real-world disordered networks may undergo deteriorated functional stability, often exhibiting discontinuous or first-order phase transition to an alternative state, as the input conditions change. Such sudden transitions in a network occur due to the inability of many nodes to cope with internal or external stresses. However, regular networks can buffer the collapse of a network state in response to increased environmental stress, overall supporting the network beyond a tipping point. Notably, the network's internal factors, such as average degree and coupling strength, can also regulate an abrupt transition. For weak interaction strengths, the change in network topology does not impact the system's resilience, while it can delay or remove the discontinuous transition in the system's state. The strong coupling can decrease the resilience of both regular as well as disordered networks. In contrast, disordered networks are robust to change in the network's average degree, as they reveal a sudden transition to an alternative state at low and high network degrees. We observe that increasing network degree decreases the resilience of the regular networks, and transitions become abrupt.

Furthermore, we find that each node's dynamics can significantly influence the response of a network's state with variations in external environmental stress. The dominance of limit cycle oscillations in the isolated components can shape the interaction network's response to changing stress. When cyclic dynamics dominate, increased coupling strength buffers the sudden transition by the emergence of fluctuations before transitioning to an alternate state. The propensity of fluctuations, however, is observed to be more for disordered networks. Thus, cyclic dynamics significantly delay the onset of a system's sudden transition to a collapsed state, and the resilience of disordered networks can be enhanced by controlling the coupling parameter and the network's average degree. We find that entirely random, ER, and BA networks share similar outcomes observed for disordered networks with small-world topology. Overall, the presence of nonequilibrium dynamics in nodes can improve network resilience by delaying sudden transitions and flickering between alternative states in the network preceding a transition can also work as an early warning signal [51].

While some networks are highly resilient to environmental stress, others show vulnerable response towards it. The nature and scale of sudden transitions in a network due to changing environmental stress can significantly owe to the diversity of network topology, internal perturbations, and external heterogeneity. Hence, we analyze early warning signals [52,53] to foresee such varying nature of transitions. We test the predictability of network-based early warning indicators for different network topologies [47] by investigating the covariance matrix of our system in the presence of additive Gaussian white noise. We observe that in the vicinity of the transition phase, the variance of the fluctuations increases. This increase is more substantial for regular than that for the other network topologies and being least for the ER network.

In a few recent studies of neuronal models real world networks are considered, for example, in Ref. [54] the authors considered the connectivity matrix based on the cat cerebral cortex and observed partial synchronization in the system. Recently, Ref. [55] explored the dynamics of FHN neurons whose connectivities are extracted from Magnetic Resonance Imaging (MRI) data and found dynamic pacemaker effect that mimics a real physiological condition. Further, [35] considered a network of FHN neurons whose connectivity was obtained from empirical diffusion tensor imaging (DTI) of healthy human brain and the authors were able to mimic epileptic-seizure-related synchronization phenomena. These studies indicate that an immediate extension of the present work is to study resilience patterns under real world network topologies. Finally, understanding network resilience and forecasting sudden transitions in the face of rapidly evolving stress can be considered as a challenging future problem.

ACKNOWLEDGMENT

P.S.D. acknowledges financial support from the Science & Engineering Research Board (SERB), Govt. of India (Grant No. CRG/2019/002402). T.B. acknowledges financial support from the SERB, Govt. of India (Grant No. CRG/2019/002632).

[1] U. Feudel, A. N. Pisarchik, and K. Showalter, Chaos **28**, 033501 (2018).
[2] M. Scheffer, S. Carpenter, J. A. Foley, C. Folke, and B. Walker, Nature **413**, 591 (2001).
[3] M. Hirota, M. Holmgren, E. H. Van Nes, and M. Scheffer, Science **334**, 232 (2011).
[4] T. M. Lenton, H. Held, E. Kriegler, J. W. Hall, W. Lucht, S. Rahmstorf, and H. J. Schellnhuber, Proc. Natl. Acad. Sci. USA **105**, 1786 (2008).
[5] T. M. Lenton, J. Rockström, O. Gaffney, S. Rahmstorf, K. Richardson, W. Steffen, and H. J. Schellnhuber, Nature **575**, 592 (2019).
[6] Y. Sharma and P. S. Dutta, Phys. Rev. E **96**, 022409 (2017).
[7] S. Sarkar, S. K. Sinha, H. Levine, M. K. Jolly, and P. S. Dutta, Proc. Natl. Acad. Sci. USA **116**, 26343 (2019).
[8] R. M. May, S. A. Levin, and G. Sugihara, Nature **451**, 893 (2008).
[9] M. Scheffer, *Critical Transitions in Nature and Society*, Vol. 16 (Princeton University Press, Princeton, NJ, 2009).
[10] B. Walker, C. S. Holling, S. R. Carpenter, and A. Kinzig, Ecol. Soc. **9** (2004).
[11] C. Folke, S. R. Carpenter, B. Walker, M. Scheffer, T. Chapin, and J. Rockström, Ecol. Soc. **15** (2010).
[12] S. Saavedra, R. P. Rohr, V. Dakos, and J. Bascompte, Nat. Commun. **4**, 2350 (2013).
[13] J. J. Lever, E. H. van Nes, M. Scheffer, and J. Bascompte, Ecol. Lett. **17**, 350 (2014).
[14] A.-L. Barabási *et al.*, *Network Science* (Cambridge University Press, Cambridge, UK, 2016).
[15] J. Gao, B. Barzel, and A.-L. Barabási, Nature **530**, 307 (2016).
[16] X. Liu, D. Li, M. Ma, B. K. Szymanski, H. E. Stanley, and J. Gao, arXiv:2007.14464.
[17] Y.-H. Eom, Phys. Rev. E **97**, 042313 (2018).
[18] S. Saavedra, D. B. Stouffer, B. Uzzi, and J. Bascompte, Nature **478**, 233 (2011).
[19] J. Jiang, Z.-G. Huang, T. P. Seager, W. Lin, C. Grebogi, A. Hastings, and Y.-C. Lai, Proc. Natl. Acad. Sci. USA **115**, E639 (2018).
[20] E. Nagaishi and K. Takemoto, R. Soc. Open Sci. **5**, 180706 (2018).
[21] J. D. Riordan and J. H. Nadeau, Am. J. Hum. Genet. **101**, 177 (2017).
[22] S. V. Buldyrev, R. Parshani, G. Paul, H. E. Stanley, and S. Havlin, Nature **464**, 1025 (2010).
[23] R. Albert, H. Jeong, and A.-L. Barabási, Nature **406**, 378 (2000).
[24] A. Vázquez and Y. Moreno, Phys. Rev. E **67**, 015101(R) (2003).
[25] E. H. van Nes and M. Scheffer, Ecology **86**, 1797 (2005).
[26] P. V. Martín, J. A. Bonachela, S. A. Levin, and M. A. Muñoz, Proc. Natl. Acad. Sci. USA **112**, E1828 (2015).

[27] H. Weissmann, N. M. Shnerb, and D. A. Kessler, Phys. Rev. E **98**, 022131 (2018).
[28] J. M. Tylianakis and C. Coux, Trends Plant Sci. **19**, 281 (2014).
[29] R. FitzHugh, Biophys. J. **1**, 445 (1961).
[30] J. Nagumo, S. Arimoto, and S. Yoshizawa, Proc. IRE **50**, 2061 (1962).
[31] A. S. Pikovsky, M. G. Rosenblum, and J. Kurths, *Synchronization. A Universal Concept in Nonlinear Sciences* (Cambridge University Press, Cambridge, UK, 2001).
[32] N. Semenova, A. Zakharova, V. Anishchenko, and E. Schöll, Phys. Rev. Lett. **117**, 014102 (2016).
[33] A. Zakharova, *Chimera Patterns in Networks: Interplay between Dynamics, Structure, Noise, and Delay* (Springer, Berlin, 2020).
[34] G. B. Ermentrout and D. H. Terman, *Mathematical Foundations of Neuroscience* (Springer-Verlag, New York, 2010).
[35] L. Ramlow, J. Sawicki, A. Zakharova, J. Hlinka, J. C. Claussen, and E. Schöll, Europhys. Lett. **126**, 50007 (2019).
[36] M. Gerster, R. Berner, J. Sawicki, A. Zakharova, A. Škoch, J. Hlinka, K. Lehnertz, and E. Schöll, Chaos **30**, 123130 (2020).
[37] I. Shepelev, D. Shamshin, G. Strelkova, and T. Vadivasova, Chaos, Solitons Fractals **104**, 153 (2017).
[38] J. Zhou, W. Yu, X. Li, M. Small, and J.-A. Lu, IEEE Trans. Neural Netw. **20**, 1679 (2009).
[39] X. Sun, Z. Liu, and M. Perc, Nonlin. Dynam. **96**, 2145 (2019).
[40] D. J. Watts and S. H. Strogatz, Nature **393**, 440 (1998).
[41] P. Erdős and A. Rényi, Publ. Math. Inst. Hung. Acad. Sci. **5**, 17 (1960).
[42] A.-L. Barabási and R. Albert, Science **286**, 509 (1999).
[43] D. J. Wilkinson, Nat. Rev. Genet. **10**, 122 (2009).
[44] L. Gammaitoni, Phys. Rev. E **52**, 4691 (1995).
[45] H. Risken, in *The Fokker-Planck Equation* (Springer, Berlin, 1996), pp. 63–95.
[46] C. Kwon, P. Ao, and D. J. Thouless, Proc. Natl. Acad. Sci. USA **102**, 13029 (2005).
[47] S. Chen, E. B. O'Dea, J. M. Drake, and B. I. Epureanu, Sci. Rep. **9**, 2572 (2019).
[48] C. Perrings, Environ. Res. Econ. **11**, 503 (1998).
[49] R. M. May, Nature **269**, 471 (1977).
[50] M. Rietkerk, S. C. Dekker, P. C. De Ruiter, and J. van de Koppel, Science **305**, 1926 (2004).
[51] R. Wang, J. A. Dearing, P. G. Langdon, E. Zhang, X. Yang, V. Dakos, and M. Scheffer, Nature **492**, 419 (2012).
[52] V. Dakos, S. R. Carpenter, W. A. Brock, A. M. Ellison, V. Guttal, A. R. Ives, S. Kéfi, V. Livina, D. A. Seekell, E. H. van Nes, and M. Scheffer, PLoS ONE **7**, e41010 (2012).
[53] M. Scheffer, S. R. Carpenter, T. M. Lenton, J. Bascompte, W. A. Brock, V. Dakos, J. van de Koppel, I. A. van de Leemput, S. A. Levin, E. H. van Nes, M. Pascual, and J. Vandermeer, Science **338**, 344 (2012).
[54] M. Santos, J. Szezech, F. Borges, K. Iarosz, I. Caldas, A. Batista, R. Viana, and J. Kurths, Chaos, Solitons Fractals **101**, 86 (2017).
[55] I. Koulierakis, D. A. Verganelakis, I. Omelchenko, A. Zakharova, E. Schöll, and A. Provata, Chaos **30**, 113137 (2020).